Preprints of the 19th World Congress
The International Federation of Automatic Control
Cape Town, South Africa. August 24-29, 2014

Nyquist stability analysis of a VSC-HVDC system using a distributed parameter DC-cable model

Y. Song * **C. Breitholtz** **

* *Chalmers University of Technology, Göteborg, SE-412 96 Sweden (e-mail: yujiao@chalmers.se).*
** *Chalmers University of Technology, Göteborg, SE-412 96 Sweden (e-mail: claesbr@chalmers.se).*

Abstract: In this paper a two terminal VSC-HVDC system embedded in a strong grid AC-environment is considered, emphasizing modeling, controllers design and small-signal stability analysis. Traditionally, DC cables are most often modeled by Π-sections, and when using them for higher frequencies or in case of transmission over long distances, approximation accuracy aspects must be considered. Here, a distributed parameter cable model, based on the damped wave equation, is used to overcome this limitation. It is shown that the VSC-HVDC system can be described by a forward transfer function cascaded with a feedback loop. The first transfer function will be different, due to which input and output variables that are considered but is in all realistic cases stable. The feedback loop, where the forward path is a rational function and the return path is a dissipative infinite dimensional system, remains the same in all cases. The stability is then analyzed, using the Nyquist criterion, in a straight forward manner. Numerical examples are given by MATLAB.

Keywords: Distributed parameter cable model, Nyquist stability criterion, VSC-HVDC system.

1. INTRODUCTION

The main purpose of the HVDC-systems (High Voltage Direct Current) invented in the 1950:th was the transmission of DC electric power over longer distances, not seldom across water, and at both terminals embedded in AC-environment. These systems were largely based on thyristor technology [Rudervall et al. (2000)]. At the end of the 1990:th the thyristor systems were gradually replaced by so called voltage source converters, VSC:s, based on recent power transistor technology [Larsson et al. (2001)].

Various aspects of these VSC-HVDC systems have been addressed by several researchers and engineers from roughly 1997. In some of these contributions focus has been on short term operation of the VSC-HVDC systems, emphasizing dynamics and control. From the system theory point of view the VSC:s involve several linear subsystems, for example PI-controllers and linear circuit elements, but also nonlinear subsystems, due to the relations between power and voltage (or current). If large changes in voltage levels, for example due to severe system faults, should be taken into account, nonlinear dynamical models must be used in analysis. A major interest has been in the dynamics close to steady state (implying sinusoidal steady state at the AC-side and constant steady state at the DC-side). Consequently linearized dynamical models then have been in focus [Svensson (1998)].

One particular aspect of linear dynamics that has drawn much attention is the system stability. Naturally, state-space models are preferred to be used. Typically the DC-cable has been modeled by one simple Π-link [Karlsson (2002), Pipelzadeh et al. (2013)]. This is often sufficient, at least when considering short cables and low frequencies. If more general results are required, for example fast system excitation caused by abrupt disturbances and perhaps in very long cables (200 - 400 km), it would be more appropriate to use a distributed parameter cable model together with state-space (or transfer function) VSC-models.

In this paper a VSC-HVDC system is modeled, comprising VSC:s and AC-side dynamics, together with a distributed parameter cable model, based on the one dimensional damped wave equation. The system is linearized around an arbitrary operational point and the resulting linear infinitely dimensional model is based on the use of transfer functions. It turns out that the system can be described by two cascaded systems: One is a forward combination of transfer functions that will be different, due to which input signal and which output signal that are considered, but always be input to output stable. The second is a feedback system, where the forward subsystem is finite dimensional and the return subsystem only depends on the infinite dimensional cable model. The stability of this feedback system, that remains the same for all combinations of input and output signals, is analyzed by use of the Nyquist criterion. Schemes and equations are deduced in the paper and some simulations in frequency domain are showed as well. The purpose is to provide a tool for small-signal analysis of the total VSC-HVDC system, including a cable model that is valid independently of the cable length or which frequencies that can be considered due to a given

cable model approximation. The focus is here on the strong AC-grid case, making some simplifications possible. However the weak-grid case can quite likely be treated by the same approach.

2. PROBLEM FORMULATION

A standard VSC-HVDC system is described by Fig. 1. It consists of two three-phase AC sources, which represent the equivalent electrical systems that are connected by the DC cable. At the AC-side of the VSC:s, the series inductances (L_1, L_2) and resistances (R_1, R_2) represent the AC reactor and the power losses in the converter. The transmission line would be interpreted as a distributed parameter model. The shunt capacitors at the terminals are denoted by C_1, C_2 respectively.

2.1 Model and Control objectives

In a standard VSC-HVDC systems, one converter station (VSC1) is assigned the duty as the DC voltage controller to secure the stability of the DC-Bus voltage; the other station (VSC2) operates as the active power controller to guarantee and balance the power exchanges [Ooi and Wang (1990)]. Besides, in each VSC, it is possible to control the reactive power or grid voltage at the AC side; this is, however, not considered in this paper.

As the DC cable is modeled by a single Π-link, the stability of the system can be investigated through the eigenvalue calculation. However, the high frequency information is not well interpreted by the Π-scheme cable model and thus impossible to analyze the real dynamic influence from the DC cable. The new standard VSC-HVDC model includes the distributed parameter cable model and formulate the transfer function into the block diagram as shown at Fig.2. Therefore, if $g_1(s)$ is a rational function of 's' and the infinite dimensional transfer function $h_1(s)$ represents a dissipative system, the feedback loop stability could be analyzed by use of the Nyquist criterion.

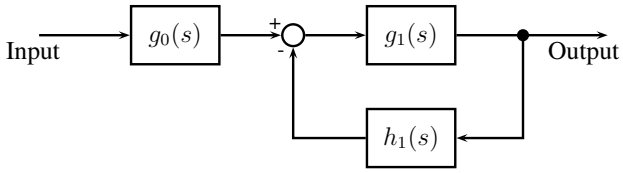

Fig. 2. General block diagram of VSC-HVDC system

2.2 Assumptions and statements

The main assumptions and statements of the proposed model are the following:

- The connected AC grids are well balanced and strong, i.e. the nominal AC grid voltage is as most subject to small variation and the dynamics of Phase Locked Loop and low pass filter for feed forward terms are ignored.
- The model is derived in the so-called dq reference plane, which is oriented according to the robust Phase Locked Loop. The dynamic transformation from three phase abc-frame into dq-frame is given by, for example, [Mohan (2001)].
- The two VSC:s are ideal and symmetrical, having a switching frequency of 1kHz. The relevant time delay is half of the switching period, around 0.5 ms. After design the system time constant is at least ten times larger then 0.5ms, the time delays of the VSC's are negligible.
- The units for voltage, current and active power are [kV], [kA] and [MW] respectively.
- All reference signals x are expressed as x^{ref}.
- The differential operator is expressed by 'p' and the Laplace form of time domain variable $x(t)$ is marked by $\tilde{x}(s)$.

3. SYSTEM MODEL

In this section, the dynamic equations of VSC is given in the power invariant dq reference frame, where the frame is chosen to be in alignment with the voltage direction i.e. $v_{sq0} = 0$. For balanced and strong AC grid, the grid frequency is assumed to be constant i.e. $\omega = 2\pi f_0$ and $f_0 = 50$Hz. Since the VSC:s are symmetric, the variables and parameters in this section would not be subscribed, i.e. index 1,2 are not used and which are applied to denote different VSC:s.

The local controller of the VSC is separated into two cascaded parts: inner current controller and outer controller. The inner current controller provides the voltage reference (v_{cd}^{ref} and v_{cq}^{ref}) to the pulse width modulator (PWM). The d-axis outer controller is used to track the reference of either DC voltage or active power and generates the d-axis current reference (i_d^{ref}) to the inner current loop. Since the q-axis current has no impact on the dynamics at the DC side (after d- and q-dynamics decoupling), the q-axis current reference (i_q^{ref}) is thus assumed to be zero.

3.1 Inner current loop

The AC current dynamics in the dq frame is given by:

$$L \cdot \frac{\mathrm{d}i_d}{\mathrm{d}t} = -R \cdot i_d + \omega L \cdot i_q + v_{sd} - v_{cd} \quad (1)$$

$$L \cdot \frac{\mathrm{d}i_q}{\mathrm{d}t} = -R \cdot i_q - \omega L \cdot i_d + v_{sq} - v_{cq} \quad (2)$$

The current controller consists of one PI-controller and two feed forward signals i.e. the grid voltage and cross coupling current, which are given as following:

$$v_{cd}^{ref} = -(K_p + \frac{K_i}{p})(i_d^{ref} - i_d) + v_{sd} + \omega L \cdot i_q \quad (3)$$

$$v_{cq}^{ref} = -(K_p + \frac{K_i}{p})(i_q^{ref} - i_q) + v_{sq} - \omega L \cdot i_d \quad (4)$$

Due to the switching action of the PWM inside the converter, a delay of half a switching period appears, where $T_{sw} = 1/(2f_{sw}) = 0.5ms$. If the design time constant of the inner current loop is chosen ten times larger than the delay T_{sw}, it is reasonable to ignore the impact of the delay during the analysis of system dynamics i.e. $v_{cd}^{ref} \approx v_{cd}$ and $v_{cq}^{ref} \approx v_{cq}$ [Harnefors et al. (2007)]. Consequently, the dynamics between the d- and q-axis are decoupled.

It is also important to notice that, in order to cancel the dominant pole $(-R/L)$ in the external circuit of the

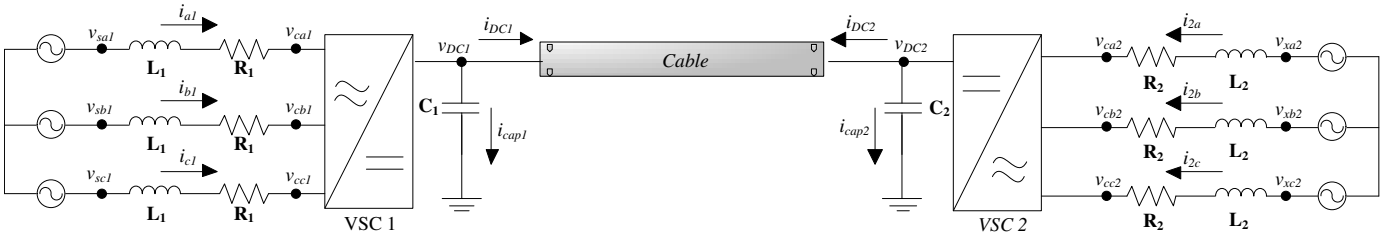

Fig. 1. Standard VSC-HVDC system embedded in a strong AC environment

converter, the PI-parameters are designed as $K_p = \alpha_c L$ and $K_i = \alpha_c R$, where α_c is the bandwidth of inner current loop and the corresponding time constant is $\tau_c = 1/\alpha_c$. The linearized inner current closed loop is then simplified as a first order system with bandwidth α_c:

$$\Delta\tilde{i}_d(s) = \underbrace{\frac{\alpha_c}{s+\alpha_c}}_{G_c(s)} \Delta\tilde{i}_d^{ref}(s) \tag{5}$$

$$\Delta\tilde{i}_q(s) = \frac{\alpha_c}{s+\alpha_c}\Delta\tilde{i}_q^{ref}(s) \tag{6}$$

Note that the unavoidable uncertainties in the AC side model parameters, L and R, from a practical point of view are assumed to be quite small. Hence these uncertainties will have only a minor impact on the inner current loop performance. In addition, since the outer loop bandwidth usually is designed to be at least ten times smaller than α_c, the effect caused by the inner loop parameter uncertainty would not influence the entire system dynamics very much. Therefore, the design of the inner current loop PI-controller based on model parameters is well justified.

However, even if the inner current feedback loop is cascaded by a slower system in the outer loop, the inner loop dynamics should not be ignored. This is due to that the inner current feedback loop performs as a low pass filter for the feed forwarded DC load power in the outer DC voltage control loop, which is shown in Fig. 3. It guarantees that no exceeded active power would be transmitted into the DC side due to high frequency resonance at the DC side.

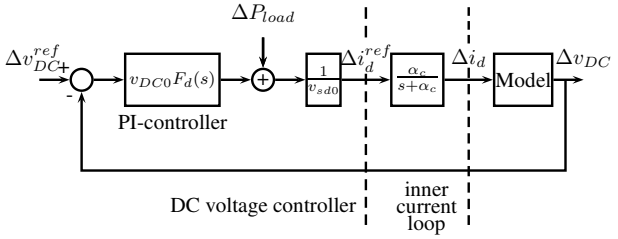

Fig. 3. DC voltage control loop (Δv_{sd} is assumed to be zero)

3.2 Direct voltage control loop

The DC voltage is determined by the capacitor charging power that is the difference between input active power to the VSC (assume the VSC is power lossless) and DC load power:

$$\frac{\mathrm{d}}{\mathrm{d}t}(\frac{1}{2}C \cdot v_{DC}^2) = P - P_{load} \tag{7}$$

$$\Rightarrow \quad C \cdot v_{DC0} \cdot \frac{\mathrm{d}\Delta v_{DC}}{\mathrm{d}t} = \Delta P - \Delta P_{load} \tag{8}$$

Therefore, the linearized expression of the input active power and DC load power are required:

$$\begin{aligned} P &= Re\{(v_{sd0} + \Delta v_{sd} + j\Delta v_{sq})(i_{d0} + \Delta i_d - ji_{q0} - j\Delta i_q)\} \\ &\approx \underbrace{v_{sd0}i_{d0}}_{P_0} + \underbrace{v_{sd0}\Delta i_d + i_{d0}\Delta v_{sd} + i_{q0}\Delta v_{sq}}_{\Delta P} \end{aligned} \tag{9}$$

$$\begin{aligned} P_{load} &= (v_{DC0} + \Delta v_{DC})(i_{DC0} + \Delta i_{DC}) \\ &\approx \underbrace{v_{DC0}i_{DC0}}_{P_{load0}} + \underbrace{v_{DC0}\Delta i_{DC} + i_{DC0}\Delta v_{DC}}_{\Delta P_{load}} \end{aligned} \tag{10}$$

(9) shows that ΔP is proportional to Δi_d and independent with Δi_q. Therefore, the output of DC voltage controller, i.e. the d-axis reference current, could be designed through the reference input active power. The reference input active power is the sum of a PI-controller operating on the error of DC voltage square and feed forward DC load power:

$$P^{ref} = \underbrace{\left(K_{pd} + \frac{K_{id}}{p}\right)}_{F_d(p)} \cdot \nu + P_{load} \tag{11}$$

$$\nu = \frac{(v_{DC}^{ref})^2 - v_{DC}^2}{2}$$

$$i_d^{ref} = \frac{P^{ref}}{v_{sd}} \tag{12}$$

$$\Rightarrow \Delta\tilde{P}^{ref} = F_d(s)v_{DC0}(\Delta\tilde{v}_{DC}^{ref} - \Delta\tilde{v}_{DC}) + \Delta\tilde{P}_{load} \tag{13}$$

$$\Delta\tilde{i}_d^{ref} = \frac{1}{v_{sd0}}\Delta\tilde{P}^{ref} - \frac{P_0}{v_{sd0}^2}\Delta\tilde{v}_{sd} \tag{14}$$

Combining equations (8-10), (13-14) and the inner current loop (5), the linearized expression of DC voltage is given as following, where Δv_{sq} is assumed to be zero (due to fast PLL dynamics):

$$\begin{aligned} \Delta\tilde{v}_{DC} = (Cv_{DC0}s + v_{DC0}F_dG_c + i_{DC0}(1-G_c))^{-1} \cdot \\ \cdot [v_{DC0}F_dG_c \cdot \Delta\tilde{v}_{DC}^{ref} - v_{DC0}(1-G_c) \cdot \Delta\tilde{i}_{DC} + \\ + i_{d0}(1-G_c) \cdot \Delta\tilde{v}_{sd}] \end{aligned} \tag{15}$$

After designing the PI-controller parameters as $K_{pd} = 2C\zeta\omega_{nd}$ and $K_{id} = C\omega_{nd}^2$, the transfer function from Δv_{DC}^{ref} to Δv_{DC} is given at (16). The approximation is based on the assumption that the inner current loop is much faster than the outer loop and thus $G_c(s) \approx 1$. However, this assumption is only used to analyze the transfer function from Δv_{DC}^{ref} to Δv_{DC} but not for the entire two terminal

VSC-HVDC system.

$$\frac{\Delta\tilde{v}_{DC}}{\Delta\tilde{v}_{DC}^{ref}} = \frac{v_{DC0}F_d(s)G_c(s)}{Cv_{DC0}s + v_{DC0}F_d(s)G_c(s) + i_{DC0}(1-G_c(s))} \approx \frac{v_{DC0}F_d(s)}{Cv_{DC0}s + v_{DC0}F_d(s)} = \frac{2\zeta\omega_{nd}s + \omega_{nd}^2}{s^2 + 2\zeta\omega_{nd}s + \omega_{nd}^2} \quad (16)$$

A common requirement of the closed loop DC voltage dynamics is to have a bandwidth ten times smaller than the inner loop [Harnefors et al. (2007)] so that the DC voltage would not be sensitive to the DC load power. In addition, the damping ratio is chosen around 1 in order to decrease the DC voltage overshoot. As $\zeta = 1$, the relation between the natural frequency ω_{nd} and the DC voltage bandwidth α_d is:

$$\omega_{nd} = \sqrt{-(2\zeta^2+1) + \sqrt{(2\zeta^2+1)^2+1}} \cdot \alpha_d \approx 0.4\alpha_d \quad (17)$$

3.3 Active power control loop

For the outer controller of transmitted active power, again a PI-controller is used. The controller parameters are designed by inner current loop pole cancelation, choosing the bandwidth of the outer loop as $\alpha_p = 0.2\alpha_d$. Therefore, the DC voltage would not display large oscillations during the variations of transmitted active power. The linearized differential equations of the active power control loop are derived as following:

$$i_d^{ref} = (K_{pp} + \frac{K_{ip}}{p})(P^{ref} - P)/v_{sd} \quad (18)$$

$$\Rightarrow \Delta\tilde{i}_d^{ref} = \frac{1}{v_{sd0}}(K_{pp} + \frac{K_{ip}}{s})(\Delta\tilde{P}^{ref} - \Delta\tilde{P}) \quad (19)$$

Combining equations (8-10), (19) and the inner current loop (5), the linearized expression of active power and DC voltage is given as following, where Δv_{sq} is assumed to be zero and $K_{pp} = \alpha_p/\alpha_c$, $K_{ip} = \alpha_p$:

$$\Delta\tilde{P} = \underbrace{\frac{\alpha_p}{s+\alpha_p}}_{G_p(s)} \cdot \Delta\tilde{P}^{ref} + \frac{i_{d0}s}{s+\alpha_p} \cdot \Delta\tilde{v}_{sd} \quad (20)$$

$$\Delta\tilde{v}_{DC} = (Cv_{DC0}s + i_{DC0})^{-1}(G_p(s)\cdot\Delta\tilde{P}^{ref} + i_{d0}(1-G_p(s))\cdot\Delta\tilde{v}_{sd} - v_{DC0}\cdot\Delta\tilde{i}_{DC}) \quad (21)$$

It can be seen from above equations that, for active power controller, the AC dynamics is independent with DC dynamics but not reversely.

3.4 DC cable

The conventional method of approximating a transmission line is to replace the line by cascaded lumped RLGC-sections, which is shown in Fig. 4. The terminal voltage and current are represented by v_{DC1}, v_{DC2}, i_{DC1} and i_{DC2}. The cable parameters are given by r, l, g, c and d, which are the cable density of resistance, inductance, conductance, capacitance and the cable length.

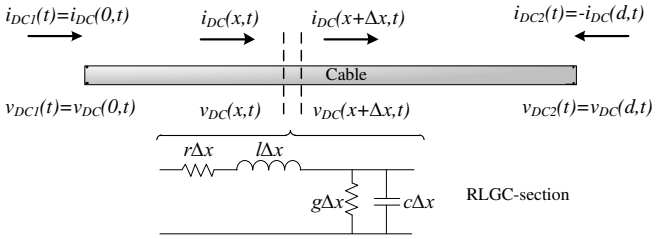

Fig. 4. DC cable model

At an arbitrary distance 'x' from terminal 1, the voltage v_{DC} and current i_{DC} obey:

$$\frac{\partial v_{DC}(x,t)}{\partial x} + r\cdot i_{DC}(x,t) + l\cdot\frac{\partial i_{DC}(x,t)}{\partial t} = 0 \quad (22)$$

$$\frac{\partial i_{DC}(x,t)}{\partial x} + g\cdot v_{DC}(x,t) + c\cdot\frac{\partial v_{DC}(x,t)}{\partial t} = 0 \quad (23)$$

These well known transmission line equations are readily derived directly from Fig. 4, after letting the element Δx approach zero. Taking the Laplace transforms of these two linear PDE:s and eliminating i_{DC}, the following ordinary differential equation is obtained:

$$\frac{\mathrm{d}^2\tilde{v}_{DC}(x,s)}{\mathrm{d}x^2} - (r+l\cdot s)(g+c\cdot s)\cdot\tilde{v}_{DC}(x,s) = 0 \quad (24)$$

The boundary conditions are:

$$\tilde{v}_{DC}(0,s) = \tilde{v}_{DC1}(s) \quad (25)$$

$$\tilde{v}_{DC}(d,s) = \tilde{v}_{DC2}(s) \quad (26)$$

Introducing the complex damping factor per unit length γ and the wave admittance Y_0:

$$\gamma(s) = \sqrt{(c\cdot s+g)(l\cdot s+r)} \quad (27)$$

$$Y_0(s) = \sqrt{\frac{c\cdot s+g}{l\cdot s+r}} \quad (28)$$

Define the current from the AC to DC side as positive, implying that the terminal currents $i_{DC1}(t) = i_{DC}(0,t)$ and $i_{DC2}(t) = -i_{DC}(d,t)$ (see Fig. 4). We can formulate a relationship between the terminal currents and voltages:

$$\begin{bmatrix}\tilde{i}_{DC1}(s)\\ \tilde{i}_{DC2}(s)\end{bmatrix} = \begin{bmatrix}h_1(s) & -h_2(s)\\ -h_2(s) & h_1(s)\end{bmatrix}\cdot\begin{bmatrix}\tilde{v}_{DC1}(s)\\ \tilde{v}_{DC2}(s)\end{bmatrix} \quad (29)$$

Further, letting $\Gamma(s) = \gamma(s)\cdot d$, the functions h_1 and h_2 are obtained as:

$$h_1(s) = Y_0(s)\coth(\Gamma(s)) \quad (30)$$

$$h_2(s) = \frac{Y_0(s)}{\sinh(\Gamma(s))} \quad (31)$$

As the cable system itself is dissipative, the functions $h_1(s)$ and $h_2(s)$ have infinite numbers of poles strictly located in the left half plane.

4. BLOCK DIAGRAM OF TWO TERMINAL VSC-HVDC SYSTEM

As previously mentioned, the VSC-HVDC system is assumed to be embedded in a strong AC environment. Here the DC cable is described by a distributed parameter model, not to be restricted to the study of short cables and low frequencies. In the control system, the converter

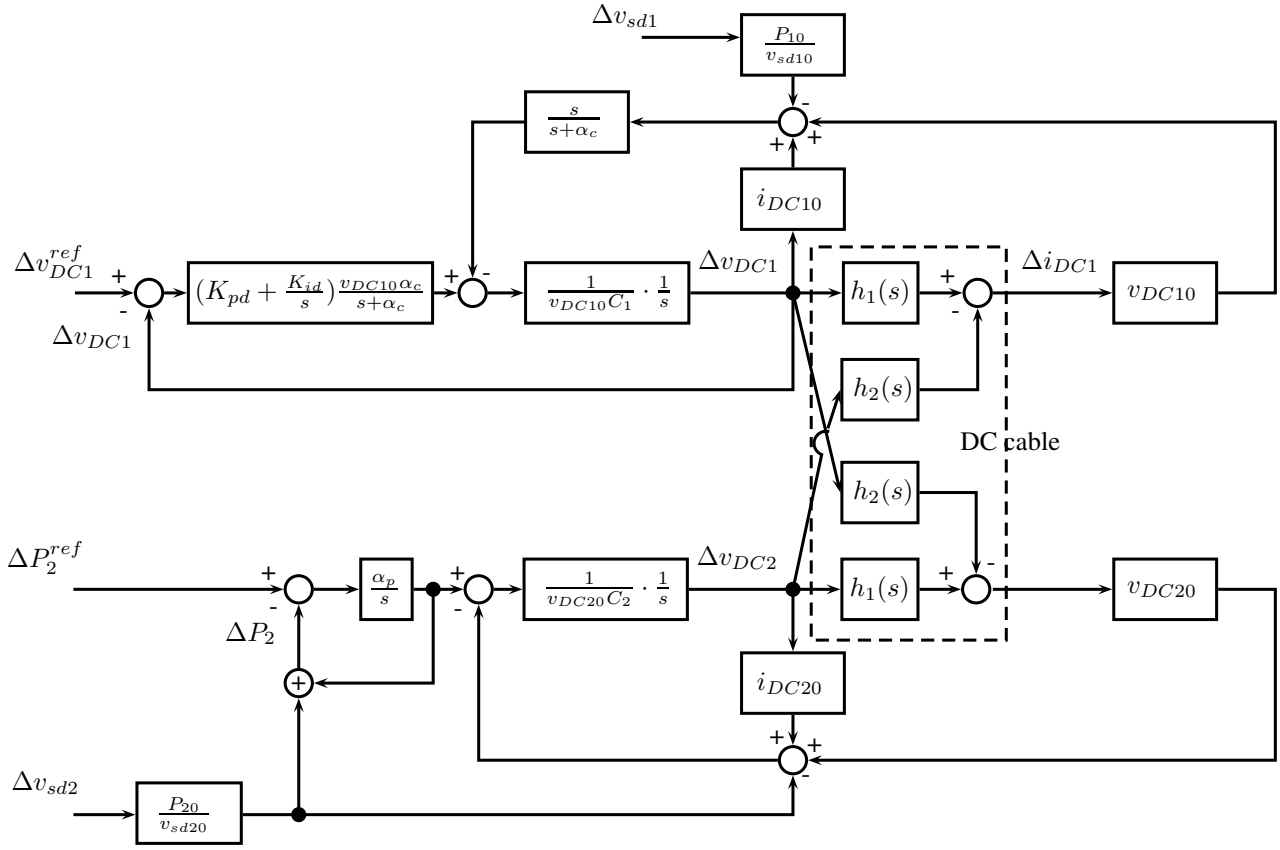

Fig. 5. Linearized VSC-HVDC system

VSC1 is assigned the duty of controlling the DC voltage and VSC2 of controlling the transmitted active power. The block diagram illustrating this case is found in Fig. 5.

In the linearized system, there are two reference signals, Δv_{DC1}^{ref} and ΔP_2^{ref}, and two AC grid disturbances, Δv_{sd1} and Δv_{sd2}, considered as inputs. From (20), it is clear that the active power ΔP_2 is independent of DC side variations and depends on the inputs ΔP_2^{ref} and Δv_{sd2}. Therefore, the DC grid voltage Δv_{DC1} and Δv_{DC2} have been chosen as the system outputs.

Use Fig. 5, rewrite equations (15), (21) and combine with the DC cable dynamics (29):

$$\Delta\tilde{v}_{DC1} = g_{11}\Delta\tilde{v}_{DC1}^{ref} + \frac{i_{d10}g_{11}s}{v_{DC10}\alpha_c F_d}\Delta\tilde{v}_{sd1} - \frac{g_{11}s}{\alpha_c F_d}\Delta\tilde{i}_{DC1} \tag{32}$$

$$\Delta\tilde{v}_{DC2} = \frac{g_{12}G_p}{v_{DC20}}\Delta\tilde{P}_2^{ref} + \frac{i_{d20}(1-G_p)g_{12}}{v_{DC20}}\Delta\tilde{v}_{sd2} - g_{12}\Delta\tilde{i}_{DC2} \tag{33}$$

$$\Delta\tilde{i}_{DC1} = h_1\Delta\tilde{v}_{DC1} - h_2\Delta\tilde{v}_{DC2} \tag{34}$$

$$\Delta\tilde{i}_{DC2} = -h_2\Delta\tilde{v}_{DC1} + h_1\Delta\tilde{v}_{DC2} \tag{35}$$

Where,

$$g_{11} = \frac{v_{DC10}F_dG_c}{C_1v_{DC10}s + v_{DC10}F_dG_c + i_{DC10}(1-G_c)} \tag{36}$$

$$g_{12} = \frac{v_{DC20}}{C_2v_{DC20}s + i_{DC20}} \tag{37}$$

Insert (34) and (35) into (32) and (33):

$$\underbrace{\begin{bmatrix} 1+\frac{g_{11}s}{\alpha_cF_d}h_1 & -\frac{g_{11}s}{\alpha_cF_d}h_2 \\ -g_{12}h_2 & 1+g_{12}h_1 \end{bmatrix}}_{\Lambda(s)}\begin{bmatrix}\Delta\tilde{v}_{DC1}\\ \Delta\tilde{v}_{DC2}\end{bmatrix} =$$

$$\underbrace{\begin{bmatrix} g_{11} & 0 & \frac{i_{d10}g_{11}s}{\alpha_cv_{DC10}F_d} & 0 \\ 0 & \frac{g_{12}G_p}{v_{DC20}} & 0 & \frac{i_{DC20}(1-G_p)g_{12}}{v_{DC20}} \end{bmatrix}}_{\Phi(s)}\begin{bmatrix}\Delta\tilde{v}_{DC1}^{ref}\\ \Delta\tilde{P}_2^{ref}\\ \Delta\tilde{v}_{sd1}\\ \Delta\tilde{v}_{sd2}\end{bmatrix} \tag{38}$$

Thus, the MIMO transfer function between inputs and outputs is given by:

$$\begin{bmatrix}\Delta\tilde{v}_{DC1}\\ \Delta\tilde{v}_{DC2}\end{bmatrix} = \Lambda^{-1}\Phi\begin{bmatrix}\Delta\tilde{v}_{DC1}^{ref}\\ \Delta\tilde{P}_2^{ref}\\ \Delta\tilde{v}_{sd1}\\ \Delta\tilde{v}_{sd2}\end{bmatrix} \tag{39}$$

Noting from (29) that the DC cable dynamics is symmetric and as $h_1^2(s) - h_2^2(s) \equiv Y_0^2(s)$, the determinant of the matrix Λ is independent of the irrational function $h_2(s)$.

In addition, this conclusion can be extended to weak AC grid or the case considering the dynamics of PLL and the low pass filter for the feed forwards at each VSC, again see [Harnefors et al. (2007)].

From what is mentioned above, it is possible to rewrite the block diagram of each input output combination into the form of Fig. 2, where $g_1(s)$ is determined by $\det(\Lambda)$ and

unique for all input output combinations. The determinant of Λ and g_1 are then given by:

$$\det(\Lambda) = \underbrace{(1 + \frac{g_{11}g_{12}s}{\alpha_c F_d} Y_0^2)}_{g_{1d}(s)} + \underbrace{(g_{12} + \frac{g_{11}s}{\alpha_c F_d})}_{g_{1n}(s)} \cdot h_1 \quad (40)$$

$$g_1(s) = \frac{g_{1n}(s)}{g_{1d}(s)} \quad (41)$$

$$\frac{1}{\det(\Lambda)} = \frac{g_1}{1 + g_1 h_1} \cdot \frac{1}{g_{1n}} \quad (42)$$

Unlike $g_1(s)$ which remains the same, $g_0(s)$ depends on which element of the MIMO transfer function $\Lambda^{-1}\Phi$ that is picked out due to choice of input and output signals. As normally $\Delta v_{DC1}^{ref} = 0$ (implying that $v_{DC1}^{ref} = v_{DC10}$), the most encountered situation is a change in the desired transmitted power ΔP_2^{ref} and its impact on the DC line voltage Δv_{DC1}. At the same time, no AC disturbances are considered. Therefore, the transfer function from ΔP_2^{ref} to Δv_{DC1} is deduced below.

4.1 Dynamics from ΔP_2^{ref} to Δv_{DC1}

The forward path function $g_0(s)$ corresponding to the input ΔP_2^{ref} and output Δv_{DC1} is:

$$g_0(s) = \underbrace{\frac{g_{11}g_{12}G_p s}{v_{DC20}\alpha_c F_d g_{1n}}}_{f_1(s)} h_2(s) \quad (43)$$

The block diagram from ΔP_2^{ref} to Δv_{DC1} is illustrated at Fig. 6, where $f_1(s)$ is a rational function with respect to 's' and $h_2(s)$ has infinite number of stable poles.

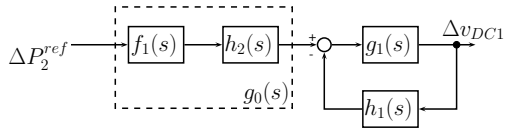

Fig. 6. Block diagram from ΔP_2^{ref} to Δv_{DC1}

Insert (36), (37) into (43), the expression of $f_1(s)$ is given as following:

$$f_1(s) = \frac{\alpha_p s}{v_{DC20}(s + \alpha_p)Q_3(s)} \quad (44)$$

$$Q_3(s) = (C_1 + C_2)s^3 + (C_1\alpha_c + \frac{i_{DC10}}{v_{DC10}} + \frac{i_{DC20}}{v_{DC20}})s^2 + \\ + \alpha_c K_{pd} s + \alpha_c K_{id} \quad (45)$$

In order to guarantee the roots of $Q_3(s)$ are located at the left half plane, the following inequality should be hold:

$$\frac{C_1\alpha_c + \frac{i_{DC10}}{v_{DC10}} + \frac{i_{DC20}}{v_{DC20}}}{C_1 + C_2} > \frac{K_{id}}{K_{pd}} = \frac{\omega_{nd}}{2\zeta} \quad (46)$$

For the purpose of less transmission losses, the DC voltage drop between two terminals should be small, which implies that $i_{DC10}/v_{DC10} + i_{DC20}/v_{DC20}$ is much less than $C_1\alpha_c$. In addition, the bandwidth of inner current loop α_c is designed to be ten times larger than the DC voltage loop. Therefore the inequality holds for all reasonable design of PI-controllers and the poles of $f_1(s)$ have strictly negative real part and are thus stable.

Similarly, it can be proved that the feed forward path function $g_0(s)$ is stable for all the input output combinations. Therefore, the entire system stability in practice only depends on the feedback loop dynamics.

5. CLOSED LOOP STABILITY ASSESSMENT

As was previously concluded, for reasonably designed PI-parameters, the entire system stability only relies on the feedback loop $g_1(s)/[1 + g_1(s)h_1(s)]$, where $g_1(s)$ is a rational function with respect to 's' and $h_1(s)$ is input to output stable. Therefore, the number of unstable poles of the open loop transfer function $g_1(s)h_1(s)$ is determined by $g_1(s)$, where $g_1(s)$ is:

$$g_1(s) = \frac{Q_3(s)(ls + r)}{P_5(s)} \quad (47)$$

$$P_5(s) = (ls + r)(C_2 s + \frac{i_{DC20}}{v_{DC20}})[C_1 s^3 + (C_1\alpha_c + \frac{i_{DC10}}{v_{DC10}})s^2 \\ + \alpha_c K_{pd} s + \alpha_c K_{id}] + s^2(cs + g) \quad (48)$$

Assuming a closed path Υ, enclosing all of the right half complex s-plane and having the clockwise positive direction, we can apply the Nyquist criterion: The number of anti-clockwise encirclements around the point (-1,0) in the $g_1(s)h_1(s)$-plane should, for a stable closed loop system, equal the number of open loop unstable poles of $g_1(s)$, as $h_1(s)$ is already a stable function [Astrom and Murray (2008)].

In the case study setup, the VSC-HVDC system parameters and initial states are listed in Table1. There are two cases that would be discussed in this section: one example is using the rectifier (AC→DC) as DC voltage controller (standard situation) and the other is using the inverter (DC→AC) as DC voltage controller.

Table 1. Parameter of VSC-HVDC system

Cable distance	d	50,150,450	km
Cable inductance density	l	0.189	mH/km
Cable capacitance density	c	0.207	μF/km
Cable resistance density	r	0.0376	Ω/km
Cable conductance density	g	0	S/km
Phase reactor inductance	L	53	mH
Phase reactor resistance	R	0.167	Ω
DC shunt capacitor	C	33	μF
Rated AC voltage (dq-frame)	v_{sd0}	200	kV
Rated DC voltage	v_{DC0}	300	kV
Rated transmission power	P_0	600	MW
System frequency	f	50	Hz

5.1 Rectifier performs as DC voltage controller

If the rectifier controls the DC voltage and the inverter controls the transmitted active power, the steady states are $v_{DC10} = 300kV$ and $P_{20} = -600MW$. The poles of $g_1(s)$ with different cable distances are given in Table 2. For all three cable distances, there is one unstable pole of the open loop transfer function $g_1(s)h_1(s)$.

The Nyquist plots of the transfer functions $g_1(j\omega)h_1(j\omega)$ with different cable distances are given in Fig. 7. It shows that for all three cases, $g_1(j\omega)h_1(j\omega)$ anti-clockwise encircles the critical point (-1,0) once, which is equal to

Table 2. Poles of $g_1(s)$ with P_{20}=-600MW

d	Poles of $g_1(s)$				
50	23.9	-3.3+3.4j	-3.3-3.4j	-206.8+954j	-206.8-954j
150	25.3	-3.3+3.5j	-3.3-3.5j	-204.5+951j	-204.5-951j
450	31.3	-3.3+3.5j	-3.3-3.5j	-194.7+938j	-194.7-938j

the number of positive poles of $g_1(s)h_1(s)$. Consequently, for the different cable distances, d=50km, 150km, 450km, the VSC-HVDC system remains stable at the operational point v_{DC10}=300kV and P_{20}=-600MW.

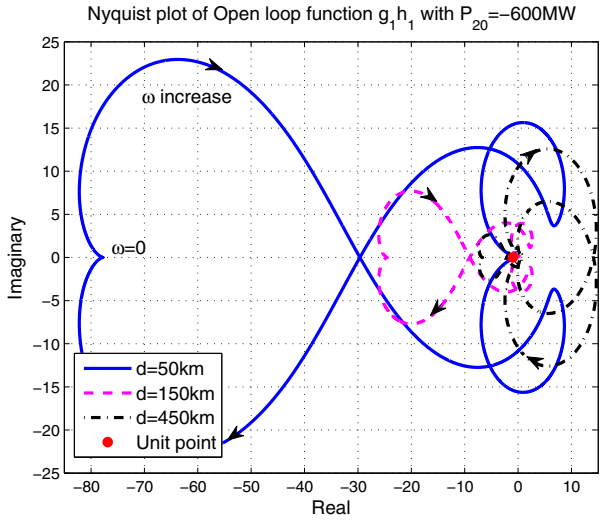

(a)Full curve of $g_1h_1(j\omega)$ with ω from $-\infty$ to ∞

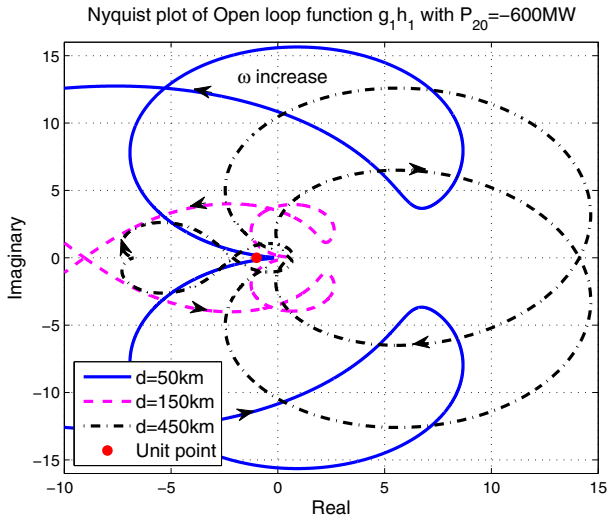

(b)Amplified curve around critical point (-1,0)

Fig. 7. Nyquist plot of $g_1h_1(j\omega)$ with $P_{20} = -600MW$: d=50km (solid blue); d=150km (dashed red); d=450km (dashed dotted black)

5.2 Inverter performs as DC voltage controller

If instead the inverter controls the DC voltage and the rectifier controls the transmitted active power, the steady states are $v_{DC10} = 300kV$ and $P_{20} = 600MW$. The poles of $g_1(s)$ with different cable distances are given in Table 3. For all three cases, there are two unstable poles of the open loop transfer function $g_1(s)h_1(s)$.

Table 3. Poles of $g_1(s)$ with P_{20}=600MW

d	Poles of $g_1(s)$				
50	1.2+11.5j	1.2-11.5j	-3.6	-198+994j	-198-994j
150	1.1+11.3j	1.1-11.3j	-3.6	-195+995j	-195-995j
450	0.95+10.6j	0.95-10.6j	-3.6	-190+996j	-190-996j

The Nyquist plots of the transfer functions $g_1(j\omega)h_1(j\omega)$ with different cable distances are given in Fig. 8. It shows that for all three cases, $g_1(j\omega)h_1(j\omega)$ anti-clockwise encircles the critical point (-1,0) twice, which is equal to the number of positive poles of $g_1(s)h_1(s)$. Consequently, for the different cable distances, d=50km, 150km, 450km, the VSC-HVDC system remains stable at the operational point v_{DC10}=300kV and P_{20}=600MW.

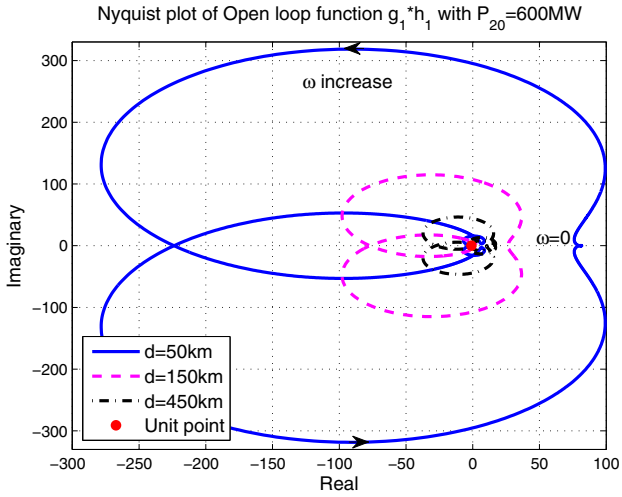

(a)Full curve of $g_1h_1(j\omega)$ with ω from $-\infty$ to ∞

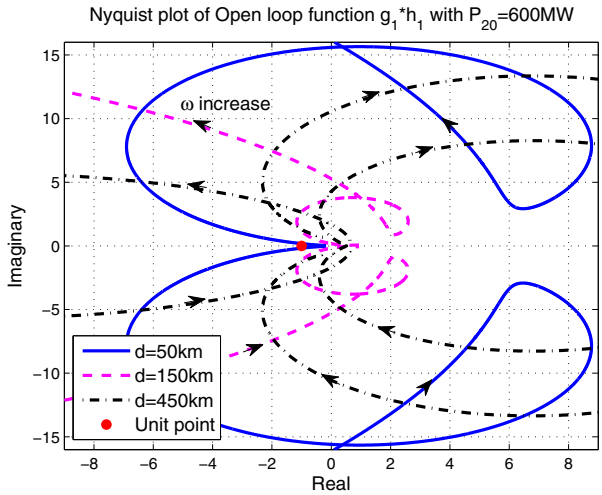

(b)Amplified curve around critical point (-1,0)

Fig. 8. Nyquist plot of $g_1h_1(j\omega)$ with $P_{20} = 600MW$: d=50km (solid blue); d=150km (dashed red); d=450km (dashed dotted black)

6. CONCLUSIONS

A mathematical model for small-signal stability analysis of a two terminal VSC-HVDC system with a distributed parameter DC cable model has been presented. Due to the

symmetric properties of the cable model, the block diagram of each input output combination could be rewritten as in Fig. 2, where $g_0(s)$ is stable with reasonable design of the DC voltage PI-controller and the forward path of the feedback loop, $g_1(s)$, is a rational function of 's' and the return path $h_1(s)$ is dissipative. Using this approach, the small-signal stability could be analyzed by the Nyquist criterion. Two examples have been illustrated, showing that in both cases with either the rectifier or the inverter working as DC voltage controller, the system is stable for three different cable distances d=50km, 150km, 450km.

The proposed method enables the VSC-HVDC system stability to be determined with arbitrary DC cable length and not limited to short length cable model approximations. Further, no assumptions of low frequency bands are demanded by using the distributed parameter cable model. The proposed approach to stability analysis could in principle be extended into the weak grid AC environment case. Some more (rational) transfer functions have then to be taken into account as well.

REFERENCES

Astrom, K.J. and Murray, R.M. (2008). *Feedback System - An Introduction for Scientists and Engineers*. Princeton university press.

Harnefors, L., Bongiorno, M., and Lundberg, S. (2007). Input-Admittance Calculation and Shaping for Controlled Voltage-Source Converters. *IEEE transactions on industrial electronics*, 54(6), 3323–3334.

Karlsson, P. (2002). *DC Distributed Power Systems - analysis, design and control for a renewable energy system*. Lund University.

Larsson, T., Edris, A., Kidd, D., Aboytes, F., and Haley, R. (2001). Eagle Pass Back-to-Back Tie : a Dual Purpose Application of Voltage Source Converter technology. *IEEE Power Enginnering Society Summer Meeting*, 3, 1686–1691.

Mohan, N. (2001). *Advanced electric drives: analysis, control and modeling using Simulink*. MNPERE.

Ooi, B. and Wang, X. (1990). Voltage angle lock loop control of the boost type PWM converter for HVDC application. *IEEE Transactions on Power Electronics*, 5(2), 229–235. doi:10.1109/63.53160.

Pipelzadeh, Y., Chaudhuri, B., and Green, T.C. (2013). Control Coordination Within a VSC HVDC Link for Power Oscillation Damping : A Robust Decentralized Approach Using Homotopy. *IEEE Transactions on Control Systems Technology*, 21(4), 1270–1279.

Rudervall, R., Charpentier, J., and Raghuveer, S. (2000). High Voltage Direct Current (HVDC) Transmission Systems Technology Review Paper. *Energy Week 2000*.

Svensson, J. (1998). *Grid-Connected Voltage Source Converter Control Principles and Wind Energy Applications*. 331. Chalmer University of Technology.